Preprints of the 2012 20th Mediterranean Conference on Control & Automation (MED), Barcelona, Spain, July 3-6, 2012



# Trajectory optimization satisfying the robot's kinodynamic constraints for obstacle avoidance

Ioannis Arvanitakis and Anthony Tzes

***Abstract*— In this article, the artificial potential field is computed for the obstacle avoidance problem of a mobile robot, using harmonic-functions. Given the maximum linear attainable velocity of the robot, equidistant points on the robot's resulting path are selected. A third-order Bézier-curve is used for time and space parameterization of each segment of the path between neighbouring points. This curve is optimized so as the robot to be capable of moving along these segments given the maximum constraints on its linear and angular velocity. A simple non–linear feedback controller is used for tracking control of the trajectory. Simulation studies indicate the efficiency of the proposed method in optimizing the robot's trajectory.**

## I. Introduction

Mobile robotics is a research field that has received significant attention over the last years, due to its numerous applications [1]. Prime examples of these applications are, but not limited to: area surveillance, exploration of unknown and potentially hazardous environments, transportation of materials, search and rescue missions. Robot navigation, defined as the robot's ability to determine its position and orientation in its reference frame followed by the planning of a path towards goal location, plays an important role in these tasks, since it is essential for the robot to avoid obstacles, while steering itself to the target area.

Algorithms for obstacle avoidance appeared as early as mid–1980s [2, 3]. Borenstein and Koren in [4], propose the use of vector field histogram which steers the robot towards the direction of low obstacle density areas; extensions and improvements have appeared in [5]. Kavraki et al. in [6] propose the creation of a graph whose nodes are collision free configurations and edges are paths between these configurations followed by the use of a query method to find a feasible path between the start and goal node. Kuffner and LaValle in [7] propose the creation of two Rapidly-exploring Random Trees (RRT) both at start and goal position, which explore free space and advance towards each other with the help of a greedy heuristic. Khatib in [8] proposes the idea of the creation of potentials from obstacles that repel the robot and potential from target that attracts it. Artificial Potential Fields (APF) have since been utilised on various applications [9] as they offer a fast and simple method for obstacle avoidance. In the recent years many advances in obstacle avoidance have been reported [10–13].

In the present case study the main novelty is the combined use of an artificial harmonic potential fields based path planner with a Bézier–curve based trajectory generation algorithm. A first rough description of the path is extracted from the path planner with the use of harmonic potential functions. The path points are then used as control points for the Bézier-curves, in order to create a smooth trajectory. Kinodynamic motion planning [14] refers to a simplified dynamic robot–motion model, in which kinematic constraints (i.e. transversal and rotational velocity bounds) are imposed. The trajectory is then inserted to a simple non–linear error dynamics controller to establish the successful tracking of the reference trajectory.

This article is structured as it follows. In Section II the artificial harmonic potential fields algorithm is presented, while in Section III the Bézier curve trajectory generation method is being presented and the error dynamics non–linear controller is mentioned. In Section IV multiple simulation results that prove the efficacy of the proposed scheme are presented, followed by concluding remarks.

## II. Artificial Harmonic Potential Fields Method

In APF the robot moves in an area due to the potential created from the obstacles and target. The obstacles repel the robot, while the target attracts it. Potential functions are chosen so as the target has a global minimum while the obstacles are maxima. By noting $U_r^i$ the repulsive potential from the *i*-th obstacle $i = 1, \ldots, o$, $U_a$ the attractive potential from the goal position, the potential of the area can be expressed as:

$$U = U_a + \sum_{i=1}^{o} U_r^i \ . \tag{1}$$

To create the desired path, the robot moves towards the global minimum of the area. To achieve this a gradient–based optimization method is utilised. Choosing the correct functions for describing the area is an arduous task [15]. On most occasions, the utilised functions create local minima in the area. If the robot path passes through these points, its motion will be stagnated; the existence of attractive stable local minima in the derived potential has been the major drawback of this theory. Various attempts to solve this problem have been proposed in the literature [16, 17] one of which is to find functions that have few unstable local minimum points [18–20].

For the present case harmonic functions have been utilised to describe the potential in the area. First mentioned in [18] as a solution to the local minima problem, a harmonic function is a twice continuously differentiable function $U$ :

The authors are with the Department of Electrical & Computer Engineering, University of Patras, Rio, Achaia–26500, Greece.

Corresponding author's email: tzes@ece.upatras.gr

978-1-4673-2529-5/12/$31.00 ©2012 IEEE

$\Re^2 \rightarrow \Re$, which satisfies Laplace's equation:

$$\nabla^2 U = \frac{\vartheta^2 U}{\vartheta x^2} + \frac{\vartheta^2 U}{\vartheta y^2} = 0 \ . \tag{2}$$

The computed harmonic function satisfies the maximum (minimum) principle, which is given by the following corollary:

*Corollary 1:* [21] Suppose $\Omega$ is bounded and $U$ is a continuous real valued function on $\Omega$ that is harmonic on $\Omega$. Then $U$ attains its maximum (minimum) values on its boundary $\partial\Omega$.

From the above corollary it can be concluded that minima or maxima appear only on the boundary $\partial\Omega$; any possible critical points within $\Omega \setminus \partial\Omega$ will only be unstable saddle points. Defining target as $P_T$ and $\Sigma = \partial\Omega \setminus P_T$ the edges of the obstacles, the Dirichlet boundary conditions can be derived for $X = (x, y) \in \Omega$ as

$$U(X \in \Sigma) = A \ , \tag{3}$$
$$U(X \in P_T) = B \ , \ A > B \ , \ A, \ B \in \Re, \tag{4}$$

where $A$ and $B$ are the upper and lower desired bounds of the potential of the area $\Omega$. By solving the partial differential equation (2), with the boundary conditions, (3,4), the potential of the area can be found. To compute the desired path a deepest gradient descent method is utilised. The *i*-th path point, $X_i$, is given from the following equation

$$X_i = X_{i-1} - \alpha_i \frac{\nabla U}{\|\nabla U\|} \ , \ i = 1, \ldots, \tilde{N} \ , \tag{5}$$

where $\alpha_i$ is the step size. In general $\alpha_i \in (0, \min_k\{H_d^i\})$ and $H_d^i$ is the Hausdorff distance [22] of the robot from the $i$-th obstacle. To be able to create an accurate path, $\alpha_i$ should be arbitrarily small.

## III. Bèzier–Curve Based Trajectory Generation

The path points, $X_i$, found from the harmonic potential fields provide a discrete description of the path. The step size from equation (5) even though is arbitrarily small, gives a discrete path. A trajectory generation algorithm must be utilised, that will meet the kinodynamic constraints imposed by the wheeled robot and transform the path into a smooth continuous curve.

### A. Robot's Kinodynamic Model

A differential drive robot is assumed with its kinematic equations be defined as:

$$\begin{bmatrix} \dot{x} \\ \dot{y} \\ \dot{\theta} \end{bmatrix} = \begin{bmatrix} \cos(\theta) & 0 \\ \sin(\theta) & 0 \\ 0 & 1 \end{bmatrix} \begin{bmatrix} \upsilon \\ \omega \end{bmatrix} \ , \tag{6}$$

where $\upsilon(\omega)$ is the tangential(angular) velocity of the robot, $x(y)$ is the horizontal(vertical) displacement, and $\theta \in [-\pi, \ \pi]$ is the heading of the robot. In a differential drive robot, its motion is directly controlled by the right $\upsilon_R$ and left $\upsilon_L$ wheel velocities of the vehicle's two motor wheels, which affect the following expressions for $\upsilon$ and $\omega$, as:

$$\upsilon = \frac{\upsilon_L + \upsilon_R}{2} \ , \tag{7}$$
$$\omega = \frac{\upsilon_R - \upsilon_L}{\lambda} \ , \tag{8}$$

where $\lambda$ is the distance between the two wheels. The velocity constraints are depended on the maximum allowable velocities of the two wheels. Given that $\upsilon_L(\upsilon_R) \in [-\upsilon_{\max}, \upsilon_{\max}]$, hard velocity bounds are:

$$\upsilon \in [-\upsilon_{\max}, \upsilon_{\max}] \ , \tag{9}$$
$$\omega \in [-\omega_{\max}, \omega_{\max}] = [-\frac{2\upsilon_{\max}}{\lambda}, \frac{2\upsilon_{\max}}{\lambda}] \ . \tag{10}$$

The feasible kinodynamic area $(\omega \times \upsilon)$ within which a differential–drive motor can operate is $(\omega \times \upsilon) = \pm\frac{2}{\lambda}(\upsilon \pm \upsilon_{\max}$; depending on the sign, the area's four boundary edges can be computed.

### B. Bèzier Curve Based Optimization

Based on the kinodynamic model of the robot (6,7,8) and its constraints, the trajectory generation method can be derived relying on Bèzier curves [23, 24]. Given $n+1$ $2D$-control points $(P_0, P_1 ... P_n)$, the $n$-th order Bèzier curve [25] is given from:

$$P(t) = \sum_{i=0}^{n} \binom{n}{i} (1-t)^{n-i} t^i P_i, \ t \in [0, 1] \ . \tag{11}$$

If the curve must be traversed in time $\tau \in [\tau_0, \tau_f]$ then $t$ is given from $t = \frac{\tau - \tau_0}{\tau_f - \tau_0}$. Bèzier curves have two distinct properties: 1) the starting and ending segment of the curve is tangent to the first $(P_0P_1)$ and last $(P_{n-1}P_n)$ edges, and 2) $P(t) \in$ convex hull$(P_0, P_1 ... P_n)$.

For this case study in order to generate a trajectory accurate relative to the initial path, a segmented trajectory is created, consisting of sequential third order Bèzier curves.

Given the path's points $X_i, \ i = 1, \ldots, N_i \ (N_i \leq \tilde{N})$, two control points $A_i^{i+1}, B_i^{i+1}$ are introduced for each $X_iX_{i+1}$ segment, as shown in Figure 1. These control points are selected as,

$$A_i^{i+1} = X_i + l_i^1 \left(X_{i+1} - X_i\right) \ , \tag{12}$$
$$B_i^{i+1} = X_{i+1} + l_i^2 \left(X_{i+1} - X_{i+2}\right) \ . \tag{13}$$

This selection ensures that each path point is $G^1$ continuous (maintains first order geometric continuity).

Equation (11) for $n = 3$ can be rewritten:

$$P(t) = (1-t)^3 X_i + 3(1-t)^2 t(X_i + l_i^1(X_{i+1} - X_i)) + 3(1-t)t^2(X_{i+1} - l_i^2(X_{i+2} - X_{i+1})) + t^3 X_{i+1} . \tag{14}$$

Using the normalised quantity $\ell_i = \frac{\|X_iA_i^{i+1}\|}{\|X_iX_{i+1}\|}$, the angle $\theta_i = \frac{\overrightarrow{X_iX_{i+1}}}{\|X_iX_{i+1}\|} \cdot \frac{\overrightarrow{X_{i+1}B_i^{i+1}}}{\|X_{i+1}B_i^{i+1}\|}$, and under the assumption that $\|X_iA_i^{i+1}\| = \|B_i^{i+1}X_{i+1}\|$, $(l_i^1 = l_i^2)$ the expression of the Bèzier curve with respect to the local coordinate system $(\text{origin}, x-\text{axis}, y-\text{axis}) = (X_{i+1}, \overrightarrow{X_iX_{i+1}}, \overrightarrow{X_{i+1}Y_i})$ is

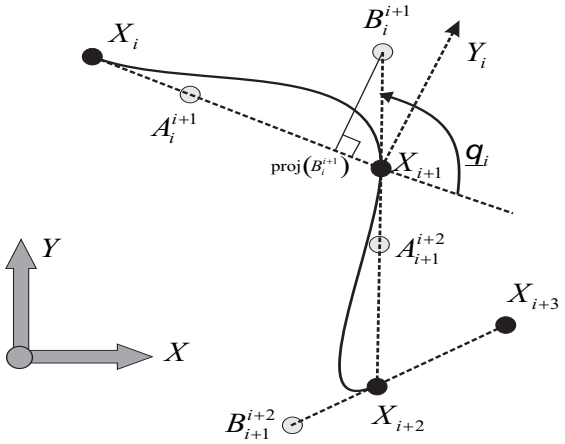


Fig. 1. Bèzier curve's control points

$$x_i(t) = -(1-t)^3 + 3(1-t)^2 t(-1+\ell_i) + 3(1-t)t^2(\ell_i \cos\theta_i) \ , \quad (15)$$

$$y_i(t) = 3(1-t)t^2(\ell_i \sin\theta_i) \ . \quad (16)$$

The length of this curve is given from,

$$L_i = \int_0^1 \sqrt{\dot{x}_i^2 + \dot{y}_i^2}\, dt \ , \text{ where} \quad (17)$$

$$\dot{x}_i^2 + \dot{y}_i^2 = 3(t-1)^2 + 3(\ell_i - 1)(3t-1)(t-1) + 3\ell_i t\cos\theta_i(3t-2)]^2 + 9\ell_i^2 t^2 \sin^2\theta_i (3t-2)^2 . \quad (18)$$

Figure 2 present the attainable length , $L_i$, of the Bèzier curve for various $\ell_i$ and $\theta_i$ parameters. It should be noted that $\max L_i \simeq 1.82$ for $\ell_i = 1$ and $\theta_i = 0$.

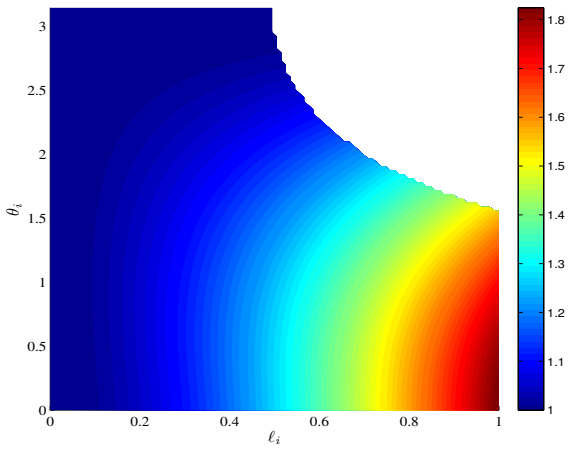


Fig. 2. Bèzier curve's length vs. $\ell_i$ and $\theta_i$ parameters

The curvature of the curve is:

$$\kappa_i = \frac{\dot{x}_i\ddot{y}_i - \dot{y}_i\ddot{x}_i}{\sqrt{\dot{x}_i^2 + \dot{y}_i^2}^3} \ , \text{ where} \quad (19)$$

$$\dot{x}_i\ddot{y}_i - \dot{y}_i\ddot{x}_i = (-18)\ell_i \sin(\theta_i)(\ell_i - 3\ell_i t + 3\ell_i t^2 - t^2) \ . \quad (20)$$

Both curve length and curvature are parameterized by angle $\theta_i$ and parameter $\ell_i$. Given the robot's velocity constraints, a kinodynamic planning must be used for the selection of parameter $\ell_i$ and the time $T_i$ needed to traverse each curve. It should be noted that the projection of the $B_i^{i+1}$ control point should be at the semi–axis $A_i^{i+1}X_{i+1}$, or

$$\overrightarrow{A_i^{i+1}\text{proj}(B_i^{i+1})} \cdot \overrightarrow{A_i^{i+1}X_{i+1}} \geq 0 \ , \quad (21)$$

in order to avoid self–loops of the Bèzier.

In general, the requirements are: 1) force the robot in traversing each segment with constant translational speed, while 2) avoiding making sharp turns. These requirements amount to: a) $0 \leq \upsilon = \frac{L_i}{T_i} \leq \upsilon_{\max}$, and b) decrease(increase) the curvature(radius) of the path, since $\omega_i(t) = \upsilon\kappa_i(t)$. However the curvature along a segment varies and the worst case corresponds to a min-max problem, where the objective is to compute a path that minimizes the maximum value of the curvature. Since the curvature depends on $\ell_i$ (given $\theta_i$) this amounts to the following optimization problem for the $\ell_i$ - selection

$$\ell_i = \arg\min\{\max|\kappa_i(t;\ell_i,\theta_i)|\} \quad (22)$$

$$\text{subject to } 0 \leq \ell_i \leq \frac{1}{1+\cos\theta_i} \ . \quad (23)$$

The constraint for this non–linear optimization problem is posed in order to avoid self–loop in the Bèzier curve. It should be noted that

$$\max_t|\omega_i(t)| = \upsilon \max_t|\kappa_i(t)| = \frac{L_i}{T_i}\max_t|\kappa_i(t)| \leq -\frac{2}{\lambda}\left(\frac{L_i}{T_i} - \upsilon_{\max}\right) , \quad (24)$$

which results to a lower bound on $T_i$.

Figure 3 presents the maximum curvature along the Bèzier curve in a logarithmic scale, $\log_{10}(\max|\kappa(t)|)$, for various $\ell_i$ and $\theta_i$ parameters.

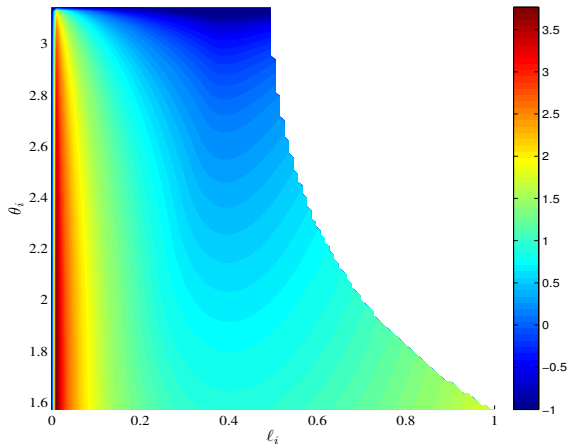


Fig. 3. Bèzier curve's maximum curvature vs. $\ell_i$ and $\theta_i$ parameters

Let the path's length from (5) be $L_p$ and assume $N_i$ control points for the Bèzier curves. If these control points are selected in an equidistant manner along the path then $L_p = N_i L_{pi}$. Large $N_i$–values lead to many segments, thus

increasing the complexity. At the same time each Bèzier curve is ensured to lay inside its convex hull defined by $(X_i, A_i^{i+1}, B_i^{i+1}, X_{i+1})$. The area of this hull is

$$\mathcal{A}_i = \frac{1}{2}\left[(X_i^x X_{i+1}^y - X_{i+1}^x X_i^y) + (X_{i+1}^x B_i^y - B_i^x X_{i+1}^y) + (B_{i+1}^x X_i^y - X_i^x B_{i+1}^y)\right] \quad (25)$$

where,$(\cdot)^x$ and $(\cdot)^y$ corresponds to the $x$- and $y$- component of the $(\cdot)$node. The larger this area, the larger the uncertainty within which each segment of the Bèzier curve resides. Another crucial factor is related to the cumulative error between: 1) the trajectory computed from the path under the assumption of constant traversing velocity and 2) the trajectory computed from each Bèzier curve. This cumulative error is expressed for the $i$-th segment as,

$$J_i = \sum_{m=1}^{\frac{T_i}{\delta T}} [(x_i(\frac{m\delta T}{T_i}) - T_p^x(iT_i + m\delta T))^2 + (x_i(\frac{m\delta T}{T_i}) - T_p^x(iT_i + m\delta T))^2] , \quad (26)$$

where $T_p(t),\ t \in [0, N_i T_i]$ corresponds to the path's point under the assumption that $T_p(0) =$ Start Point , $T_p(N_i T_i) =$ Final Point and the path is traversed with constant velocity.

The overall cost is formulated as

$$J = w_1 N_i + w_2 \sum_{j=1}^{N_i} \mathcal{A}_j + w_3 \sum_{j=1}^{N_i} T_j , \quad (27)$$

where $w_i$ are positive weights. The selection of the number of discretized nodes, $N_i$, is related to this multi term cost function, with contradicting terms, since large $N_i$ leads to smaller $\mathcal{A}_j$ and possible small $J_i$.

### C. Mobile Robot Trajectory Tracking Control

The trajectory planner provides for each segment the $x_i^r(t)$, $y_i^r(t)$, and the heading $\theta_i^r(t) = \arctan 2(\dot{y}_r(t), \dot{x}_r(t))$, where the '$r$' superscript has been added to demote the reference signal. Assume the location of the robot be $(x(t), y(t), \theta(t))$ as shown in Figure 4. The resulting errors

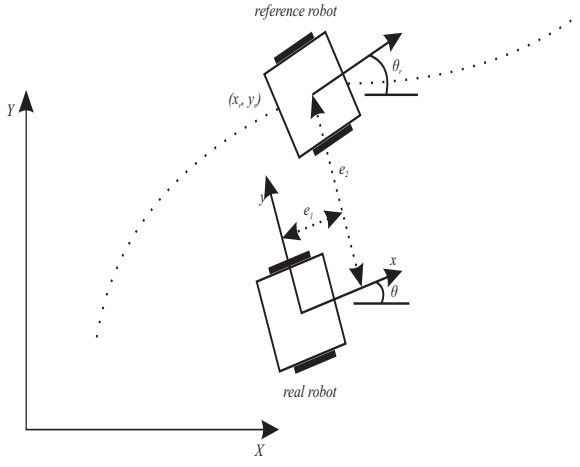


Fig. 4. Relative Kinematic (position-orientation) Errors

expressed w.r.t. the Body Fixed Frame of the mobile robot is

$$\begin{bmatrix} e_1 \\ e_2 \\ e_3 \end{bmatrix} = \begin{bmatrix} \cos\theta(t) & \sin\theta(t) & 0 \\ -\sin\theta(t) & \cos\theta(t) & 0 \\ 0 & 0 & 1 \end{bmatrix} \cdot \begin{bmatrix} x_r(t) - x(t) \\ y_r(t) - y(t) \\ \theta_r(t) - \theta(t) \end{bmatrix} . \quad (28)$$

The error kinodynamics is

$$\begin{bmatrix} \dot{e}_1 \\ \dot{e}_2 \\ \dot{e}_3 \end{bmatrix} = \begin{bmatrix} 0 & (v_i\kappa_i(t) - u_2) & 0 \\ -(v_i\kappa_i(t) - u_2) & 0 & 0 \\ 0 & 0 & 0 \end{bmatrix} \begin{bmatrix} e_1 \\ e_2 \\ e_3 \end{bmatrix} + \begin{bmatrix} 0 \\ \sin(e_3) \\ 0 \end{bmatrix} v_i + \begin{bmatrix} 1 & 0 \\ 0 & 0 \\ 0 & 1 \end{bmatrix} \begin{bmatrix} u_1 \\ u_2 \end{bmatrix} .$$

The controller

$$\begin{bmatrix} u_1 \\ u_2 \end{bmatrix} = \begin{bmatrix} -2\zeta\omega_n(t) & 0 & 0 \\ 0 & -\gamma v_i(t) & -2\zeta\omega_n(t) \end{bmatrix} \begin{bmatrix} e_1 \\ e_2 \\ e_3 \end{bmatrix} , \quad (29)$$

where $\omega_n(t) = v_i\sqrt{\kappa_i^2(t) + \gamma}$, places the poles of the error dynamics [26] at $s_1 = -2\zeta\omega_n(t)$ and $s_{2,3} = -\zeta\omega_n(t) \pm \omega_n\sqrt{\zeta^2 - 1}$.

## IV. Simulation Studies

The efficacy of the proposed scheme has been examined two different simulation studies with a robot having $v_{\max} = 0.5\ m/\sec$ and $\omega_{\max} = 3\ rad/\sec$. $\Omega$ is a square area of $225m^2$, $A = 1$ at $\partial\Omega$ and on the boundary of the obstacles, $B = 0$ at the target $P_T = (8, 7)$ while the robot is initially at $X(0) = (3, 12)$. The scattered obstacles inside $\Omega$, along with iso-contours of the potential $U$ and the generated path from (5) is shown in Figure 5. For the

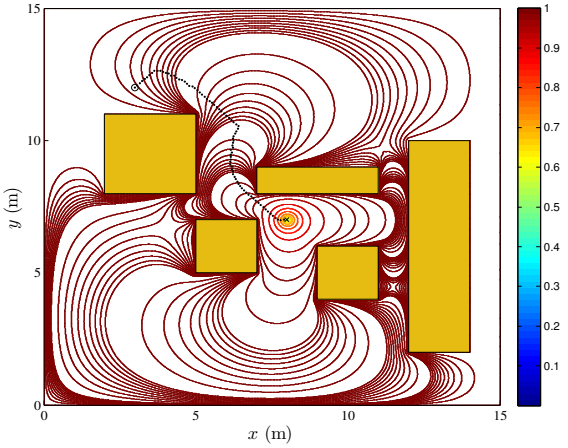


Fig. 5. Artificial Harmonic Potential Field and Generated Path ($N_i = 84$)

computation of the trajectory $N_i = 84$ control points were selected while the path could be traversed in $T_P = 38\,\sec$. The resulting trajectory is virtually on top of the path, while the robot's controller manages to track the trajectory. The convex hull of the attainable tangential and angular velocity from all Bèzier curves appears in Figure 6, which is within the feasible area. For the case of a smaller $N_i$ ($N_i = 5$), the

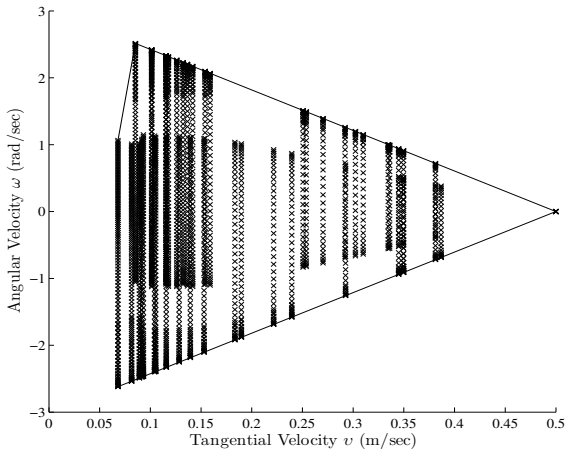


Fig. 6. Robot's attainable angular and tangential velocity

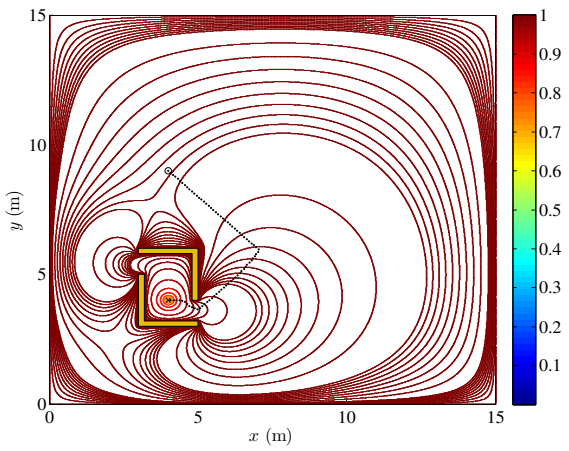


Fig. 8. Artificial Harmonic Potential Field and Generated Path ($N_i = 77$)

resulting path along with the convex hulls of each Bèzier segment appears in Figure 7. In the second case, concave

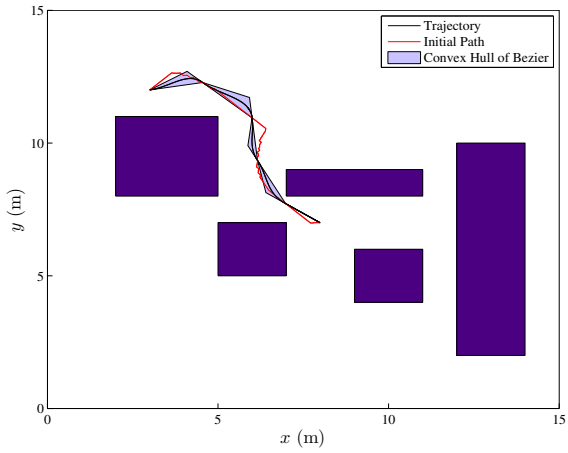


Fig. 7. Generated path and convex hulls of Bèzier curves ($N_i = 5$)

polygons surround the target $P_T = (4, 4)$. The robot is initially at $X(0) = (4, 9)$ and the potential's iso-contours and the generated path appear in Figure 8. It should be noted that in this case, if typical non–harmonic fields are used with $U_a = -\frac{K_a}{(x_t-x_r)^2+(y_t-y_r)^2}$, and $U_r^i = \frac{K_r^i}{H_d^i}$, with $K_a,\ K_r^i$ gain parameters, then the robot's path stops at the local minimum $(4, 6)$. For the case of $N_i = 8$, the reference trajectory and the robot's trajectory appear in Figure 9, where a close match is shown between these two. The resulting cost with $w_i = 1,\ i = 1, 2, 3$ is equal to $J = 79.9$ for $N_i = 77$ and $J = 53.5$ for $N_i = 8$, while the attainable convex hull of the tangential and angular velocity appear in Figure 10.

## V. Conclusions

In this paper a mobile robot navigation method based on harmonic potential functions and Bèzier curves has been presented. The proposed scheme utilises the harmonic potential function path planner to extract a rough description of

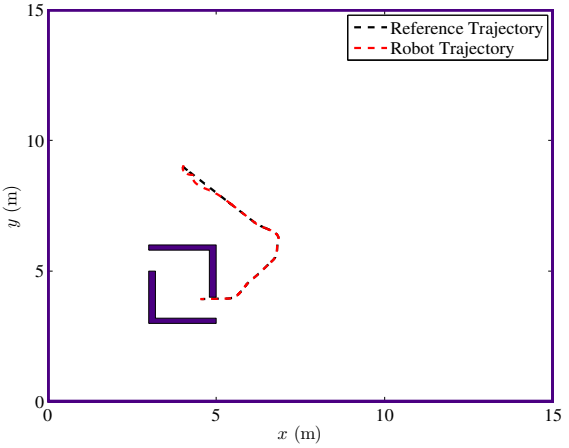


Fig. 9. Reference and Attainable Robot Trajectory

the path and then utilizes Bèzier curves to create a smooth trajectory and ensure that the robot tangential and angular velocity is within their kinodynamic constraints. The efficacy of the proposed scheme is tested in simulation studies for two environments.

## References


[1] E. Garcia, M. Jimenez, P. De Santos, and M. Armada, "The evolution of robotics research," *Robotics Automation Magazine, IEEE*, vol. 14, no. 1, pp. 90 –103, March 2007.

[2] S. M. LaValle, *Planning Algorithms*. Cambridge, U.K.: Cambridge University Press, 2006.

[3] H. Choset, K. M. Lynch, S. Hutchinson, G. Kantor, W. Burgard, L. E. Kavraki, and S. Thrun, *Principles of Robot Motion: Theory, Algorithms, and Implementations*. Cambridge, U.K.: MIT Press, 2005.

[4] J. Borenstein and Y. Koren, "The vector field histogram-fast obstacle avoidance for mobile robots," *Robotics and Automation, IEEE Transactions on*, vol. 7, no. 3, pp. 278 –288, June 1991.

[5] L. Zhang, S. LaValle, and D. Manocha, "Global vector field computation for feedback motion planning," in *Robotics and Automation, 2009. ICRA '09. IEEE International Conference on*, May 2009, pp. 477 –482.

[6] L. Kavraki, P. Svestka, J.-C. Latombe, and M. Overmars, "Probabilistic roadmaps for path planning in high-dimensional configuration spaces,"

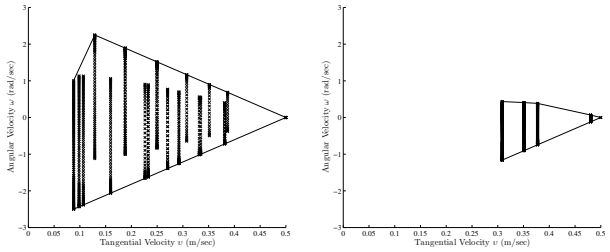


Fig. 10. Robot's attainable tangential and linear velocities

*Robotics and Automation, IEEE Transactions on*, vol. 12, no. 4, pp. 566 –580, Aug 1996.

[7] J. Kuffner, J.J. and S. LaValle, "RRT-connect: An efficient approach to single-query path planning," in *Robotics and Automation, 2000. Proceedings. ICRA '00. IEEE International Conference on*, vol. 2, 2000, pp. 995 –1001 vol.2.

[8] O. Khatib, "Real-time obstacle avoidance for manipulators and mobile robots," in *Robotics and Automation. Proceedings. 1985 IEEE International Conference on*, vol. 2, Mar 1985, pp. 500 – 505.

[9] H. Igarashi and M. Kakikura, "Path and posture planning for walking robots by artificial potential field method," in *Robotics and Automation, 2004. Proceedings. ICRA '04. 2004 IEEE International Conference on*, vol. 3, 26 April - 1 May 2004, pp. 2165 – 2170 Vol.3.

[10] C. Qixin, H. Yanwen, and Z. Jingliang, "An evolutionary artificial potential field algorithm for dynamic path planning of mobile robot," in *Intelligent Robots and Systems, 2006 IEEE/RSJ International Conference on*, Oct. 2006, pp. 3331 –3336.

[11] A. Ahmadzadeh, A. Jadbabaie, G. Pappas, and V. Kumar, "Elastic multi-particle systems for bounded-curvature path planning," in *American Control Conference, 2008*, June 2008, pp. 5035 –5040.

[12] A. Ahmadzadeh, N. Motee, A. Jadbabaie, and G. Pappas, "Multi-vehicle path planning in dynamically changing environments," in *Robotics and Automation, 2009. ICRA '09. IEEE International Conference on*, May 2009, pp. 2449 –2454.

[13] N. E. Du Toit and J. W. Burdick, "Robot motion planning in dynamic, uncertain environments," *Robotics, IEEE Transactions on*, vol. PP, no. 99, pp. 1 –15, 2011.

[14] B. Donald, P. Xavier, J. Canny, and J. Reif, "Kinodynamic motion planning," *J. ACM*, vol. 40, no. 5, pp. 1048–1066, Nov. 1993.

[15] J. Ren, K. McIsaac, R. Patel, and T. Peters, "A potential field model using generalized sigmoid functions," *Systems, Man, and Cybernetics, Part B: Cybernetics, IEEE Transactions on*, vol. 37, no. 2, pp. 477 –484, April 2007.

[16] M. Mabrouk and C. McInnes, "Solving the potential field local minimum problem using internal agent states," *Robotics and Autonomous Systems*, vol. 56, no. 12, pp. 1050 – 1060, 2008.

[17] J. Antich and A. Ortiz, "Extending the potential fields approach to avoid trapping situations," in *Intelligent Robots and Systems, 2005. (IROS 2005). 2005 IEEE/RSJ International Conference on*, Aug. 2005, pp. 1386 – 1391.

[18] J.-O. Kim and P. Khosla, "Real-time obstacle avoidance using harmonic potential functions," *Robotics and Automation, IEEE Transactions on*, vol. 8, no. 3, pp. 338 –349, Jun 1992.

[19] P. Vadakkepat, K. C. Tan, and W. Ming-Liang, "Evolutionary artificial potential fields and their application in real time robot path planning," in *Evolutionary Computation, 2000. Proceedings of the 2000 Congress on*, vol. 1, 2000, pp. 256 –263 vol.1.

[20] Y. Wang and G. Chirikjian, "A new potential field method for robot path planning," in *Robotics and Automation, 2000. Proceedings. ICRA '00. IEEE International Conference on*, vol. 2, 2000, pp. 977 –982 vol.2.

[21] S. Axler, P. Bourdon, and R. Wade, *Harmonic Function Theory*. New York, U.S.: Springer - Verlag, 2001.

[22] R. T. Rockafellar and R. J.-B. Wets, *Variational Analysis*. New York, USA: Springer, 1998.

[23] T. Fraichard and A. Scheuer, "From reeds and shepp's to continuous-curvature paths," *Robotics, IEEE Transactions on*, vol. 20, no. 6, pp. 1025 – 1035, Dec. 2004.

[24] K. Yang and S. Sukkarieh, "An analytical continuous-curvature path-smoothing algorithm," *Robotics, IEEE Transactions on*, vol. 26, no. 3, pp. 561 –568, June 2010.

[25] G. Farin, *Curves and Surfaces for CAGD, Fifth Edition: A Practical Guide*. San Francisco, CA, USA: Morgan Kaufmann Publishers Inc., 2001.

[26] G. Klancar, D. Matko, and S. Blazic, "Mobile robot control on a reference path," in *Intelligent Control, 2005. Proceedings of the 2005 IEEE International Symposium on, Mediterrean Conference on Control and Automation*, June 2005, pp. 1343 –1348.